Available online at www.sciencedirect.com
SCIENCE DIRECT®
Journal of Solid State Chemistry 178 (2005) 1030–1037
JOURNAL OF SOLID STATE CHEMISTRY
www.elsevier.com/locate/jssc

Study on antimony oxide self-assembled inside HZSM-5

Bin Li, Shijie Li, Yingxia Wang, Neng Li*, Xiyao Liu, Bingxiong Lin

College of Chemistry and Molecular Engineering, Institute of Physical Chemistry, Peking University, Number 5, Yiheyuan Road, Haidian District, Beijing 100871, PR China

Received 20 August 2004; received in revised form 29 November 2004; accepted 10 December 2004

Abstract

Sb/ZSM-5 was obtained by solid-state reaction with the mixture of Sb_2O_3 and zeolite HZSM-5 under a dry nitrogen flow at 773 K. Characterization of the treated zeolite was undertaken with XRD, ^{27}Al MAS NMR, BET, TGA and FT-IR. The results revealed that part of the antimony oxides migrated into the channels of zeolite, and decreased the Brönsted acid sites in Sb/ZSM-5 remarkably. The other part of antimony oxides together with the amorphous alumino-silicate in the products distributed on the external surface of zeolite ZSM-5 and modified it, while the framework of ZSM-5 in crystal phase was retained. The structure of occluded antimony oxide inside the channels of ZSM-5 was studied by XRD Rietveld method. The result showed that their structure can be described as a chain of non-perfect $[Sb_5O_5(H_2O)_2]_n^{5n+}$, which is parallel to the straight channel of ZSM-5. There is about 0.6 $[Sb_5O_5(H_2O)_2]^{5+}$ unit in every cell of the ZSM-5 on an average.

Keywords: Antimony oxide; Zeolite HZSM-5; Self-assembled; XRD Rietveld method; Chain of non-perfect $[Sb_5O_5(H_2O)_2]_n^{5n+}$

1. Introduction

Zeolite ZSM-5 [1] is widely used in petrochemical process due to its unique channel structures and high thermal and hydrothermal stabilities, and the structure of its framework is well studied [2,3]. As early as 1980s last century, the distribution of metal cations inside the channels of ZSM-5 by ion exchange was studied [4,5]. At the same time, a number of researchers [6–14] have been studied solid-state reaction between oxides and zeolites. The modification of zeolites with oxides, such as Sb_2O_3, MoO_3, V_2O_5 etc., has taken considerable attention by Thoret [11–14]. The authors showed that the metal cations migrate to cationic sites, where they are coordinately unsaturated. Li et al. [15] first reported that modification of Zeolite ZSM-5 with antimony oxide could enhance para-selectivity of methylation of toluene by methanol. Recently, Zheng et al. [16] studied antimony oxide-modified Zeolite ZSM-5 systemically by in situ Raman, IR spectroscopy, ^{27}Al NMR, XRD and sorption of probe molecules. They found that antimony oxide could be dispersed on the outside and inside the pores of ZSM-5 by solid-state reaction, that is, the main fraction of antimony oxide deposited on the external surface of the zeolite crystals, while a small amount of this oxide penetrated into the pores of zeolite and reacted with bridge-hydroxyl groups. They suggested that the Sb_4O_6 subunits were partially decomposed during the solid-state reaction of antimony oxide with the hydroxyl groups located on the external surface and in the pore mouth region of the zeolite. Smaller antimony oxide clusters formed subsequently entered into the zeolite pores and reacted with the bridge-hydroxyl groups. However, the structure and distribution of the metal oxides inside zeolite ZSM-5 after solid-state reaction are still not clear.

In an effort to develop a more systematic understanding of the structure of antimony oxide clusters inside the channels of zeolite ZSM-5, antimony oxide self-assembled inside ZSM-5 was investigated in this paper. The special attention was focused on the

*Corresponding author. Fax: +86 10 6275 4139.
E-mail address: lineng@pku.edu.cn (N. Li).

0022-4596/$ - see front matter © 2004 Elsevier Inc. All rights reserved.
doi:10.1016/j.jssc.2004.12.023

structure and distribution of antimony oxide species inside the channels of zeolite ZSM-5.

2. Experimental

2.1. Synthesis and chemical analysis

HZSM-5 with Si/Al ratio of 19 (Catalyst Plant of the Nankai University) was used as parent material. Pure antimony oxide (AR) was physically mixed with zeolite in a ratio of 1:9 (wt). The mixture was grounded fully and then retained in a quartz tube in a dry nitrogen flow (40 ml/min) at room temperature for 4 h, followed by raising temperature at a rate of 30 K/min to 773 K, at last, calcined at this temperature for 2 h. The obtained sample was named Sb/ZSM-5. The as-prepared Sb/ZSM-5 exposed to the environment that the relative humidity was 30–40% (condition of XRD experiment) over 24 h before analysis and characterization. The contents of Sb, Na and Si/Al ratio of the sample Sb/ZSM-5 were determined by chemical analysis. The contents of Sb and Na are 8.07 and 0.09 wt%, respectively, and the Si/Al ratio is 18.9.

2.2. Determination of the HZSM-5 crystallinity by XRD

The crystallinity of parent HZSM-5 was determined by XRD amorphous intensity card [17].

According to the quantitative analysis equation of powder XRD [2], there are relations:

$$I_a = (K_a X_a)/(\rho_a \mu_m^*), \quad (1)$$

$$I_c = (K_c X_c)(\rho_c \mu_m^*), \quad (2)$$

where I_a is the reflection intensity of amorphous phase; I_c is a reflection intensity of crystal phases; K_a and K_c are experimental constant which depended on the experimental condition and the character of the samples, and K_c is also related to the reflection *hkl* of the samples; ρ_a and ρ_c are the density of the amorphous and crystal phase of the sample, respectively; X_a and X_c are the weight percent of the amorphous and crystal phase of the sample, respectively; X_c is called crystallinity, μ_m^* is the mass absorption coefficient of the sample.

To minimize the measure error, I_c in Eq. (2) could be replaced by ΣI_c which is the sum of many reflection intensities. So,

$$\Sigma I_c = (\Sigma K_c X_c)/(\rho_c \mu_m^*) \quad I_a/\Sigma I_c = K(X_a/X_c),$$

$$1/X_c - (1/K)(I_a/\Sigma I_c) = 1, \quad (3)$$

where $K = (K_a \rho_a)/(\Sigma K_c \rho_c)$.

When the K is known, the I_a and ΣI_c could be obtained from the results of the XRD experiment, then the crystallinity of the sample (X_c) should be found.

2.2.1. Measurement of the ΣI_c

When Cu$K\alpha$ radiation was used in the experiment, we could use the all reflection intensity of crystal phase in range of 17.4–21.3° 2θ and in range of 27.7–30.8° 2θ. The sum of these peak areas is ΣI_c.

2.2.2. Measurement of the I_a

The amorphous intensity card made by us was used to determine the I_a. The following statements are the work steps:

Firstly, we collect the XRD data of the amorphous alumino-silicate oxides with Si/Al ratio closed to the ZSM-5 zeolite in the range of 5–135° 2θ.

Secondly, collect the XRD data of the perfect crystalline of α-SiO_2 (5–15 μm) in the range of 5–135° 2θ. Make sure the background.

Thirdly, extend the amorphous peaks along the shape until it intersects the background of α-SiO_2 at certain point.

Fourthly, deduct the background and get the profiles of the intensity distribution of amorphous phase (I_a).

At last, divide the reflection intensities by ten equal parts in equal interval along axis 2θ, then, connect the equal points by a curve. So, there are ten curves, and each curve covers a certain area above the α-SiO_2 background. Take the peak areas as corresponding intensity (I_a) of an amorphous phase.

Therefore, ten intensity distribution diagrams with the same peak shape but different areas were obtained. The diagram is the measure of an amorphous phase named "the amorphous intensity card".

For determining the crystallinity of the sample, we put the XRD pattern of the sample over the amorphous intensity card, and make sure the same 2θ angle and base lines just at the same position. Then, based on the lowest peak valley position to record the I_a value of the sample.

2.2.3. Determination of the value of the K

The value of K is determined by the results of the X-ray diffraction (XRD) of five mixtures, dealing with the linear least-square method.

Five samples, which the ratios of high crystallinity HZSM-5 to amorphous alumino-silicate oxides were 100:0, 95:5, 90:10, 85:15 and 80:20 (wt), respectively, were prepared. The Si/Al ratio of the sample is close to the HZSM-5.

According to Eq. (3), there is a equation group as follows:

$$1/X_c - (1/K)(I_a/\Sigma I_c)_1 = 1,$$
$$(1/0.95)(1/X_c) - (1/K)(I_a/\Sigma I_c)_2 = 1,$$
$$(1/0.90)(1/X_c) - (1/K)(I_a/\Sigma I_c)_3 = 1,$$
$$(1/0.85)(1/X_c) - (1/K)(I_a/\Sigma I_c)_4 = 1,$$
$$(1/0.80)(1/X_c) - (1/K)(I_a/\Sigma I_c)_5 = 1.$$

According to the equation group, the value of K could be carried out with the linear least-square method, if we have I_a and ΣI_c values.

At given experimental condition, the XRD patterns of the five samples was collected from 16° to 32° 2θ. Subsequently, the values of I_a and ΣI_c could be obtained by using the XRD patterns and the amorphous intensity card.

2.2.4. Determination of the HZSM-5 crystallinity

The crystallinity of HZSM-5 was determined with the above method. The diffraction data were collected from 16° to 32° 2θ, and the other conditions were the same as 2.3 below. The values of the K and the X_c were 4.79 and 91 wt%, respectively.

2.3. X-ray powder diffraction

X-ray powder diffraction data for phase analysis were collected with Rigaku D/max-rA diffractometer using Cu$K\alpha$ radiation and graphite monochromator under conditions 40 kV, 100 mA in range of 5–50° 2θ.

2.4. ^{27}Al MAS NMR

MAS NMR spectroscopy was performed on a Varian Infinityplus-400 spectrometer. The ^{27}Al NMR was measured at resonant frequency 104.3 MHz under different spinning speeds (10–12 k Hz).

2.5. BET surface area

The surface area of the samples was measured by N_2 adsorption at 77.3 K with a Micromeritics ASAP 2010 apparatus. The microporous volume was calculated from t-plot method.

2.6. Thermogravimetric analysis

Thermogravimetric analysis (TGA) of the Sb/ZSM-5 was carried out in TG 7 & DSC 7 thermal analyzer (Perkin Elmer Co.). The measurement employed the as-prepared Sb/ZSM-5 exposed to the environment when loaded in the TGA holder. The measurement was done in nitrogen at 5 K/min heating rate from 325 to 787 K, followed by recooling to room temperature. The sample weighed around 20 mg.

2.7. FT-IR

IR spectrum was recorded by NEXUS FT-IR spectrometer (NICOLET Co., USA) using a self-supporting wafer. The sample was evacuated at 573 K for 4 h in the cell at 10^{-4} mbar and then dosed with an excess of pure pyridine vapor. IR spectra of adsorbed pyridine of the samples were recorded after degassing the excess pyridine or weakly adsorbed species at 373–573 K.

2.8. Data collection and structure refinement

The data for structure analysis were collected from 5° to 80° 2θ, with a step size of 0.02° 2θ and 10 s/step under conditions Cu$K\alpha$ radiation and graphite monochromator, 40 kV, 160 mA in Rigaku D/max-rA diffractometer. The XRD intensities were recorded by a scintillation counter. The known structural parameters for the framework of ZSM-5 could be used as initial parameters [3]. Then the structure analysis was refined by Fullprof 2000 program [18]. LeBail Fitting was performed first to get suitable parameters for peaks function, and at the meantime the lattice parameters and zero point were refined. After the structure of zeolite ZSM-5 was involved, the thermal factors were refined at the first stage and they are kept unchanged during the final refinement. Then Fourier maps and population refinements gave the location of the antimony atoms sites and oxygen atoms sites. Soft constrains on distances of Si–O and Si–Si were used during the refinement. The details of crystallographic data and results of Rietveld analysis for Sb/ZSM-5 are listed in Table 1. Table 2 showed the final results of refined atomic parameters. The Si (Al)–O bond lengths of the ZSM-5 framework in Sb/ZSM-5 are summarized in Table 3.

Table 1
Crystallographic data and results of Rietveld method analysis for Sb/ZSM-5

Crystal system	Orthorombic
Space group	*Pnma* (No. 62)
a (Å)	20.1682(7)
b (Å)	19.9776(7)
c (Å)	13.4495(5)
Wavelength	Cu$K\alpha$, $K\alpha1 = 1.5406$ Å, $K\alpha2 = 1.5443$ Å $I(K\alpha2)/I(K\alpha1) = 0.5$
Range 2θ (deg)	5–80
Step width 2θ (deg)	0.02
Number of points	3750
Number of restraints	144
Number of structural variables	122
Peak profile	Split pseudovoight
Background correction	Linear interpolation of background points
R_F	*0.056*
R_{Bragg}	*0.050*
R_p	*0.099*
R_{wp}	*0.100*
R_{exp}	*0.061*
Distance restraints	
d(Si–Si)	3.10(5)
d(Si–O)	1.60(2)
d(O–O)	2.62(5)

Table 2
Positional, thermal, and population parameters for Sb/ZSM-5

Atom	X	Y	Z	Population parameters	Wyckoff. Pos.	U
T(1)	0.4241(2)	0.0589(3)	−0.3326(4)	8.0	8*d*	2.4(1)
T(2)	0.3119(3)	0.0318(3)	−0.1832(4)	8.0	8*d*	2.4(1)
T(3)	0.2776(3)	0.0641(3)	0.0319(4)	8.0	8*d*	2.4(1)
T(4)	0.1212(3)	0.0605(3)	0.0274(4)	8.0	8*d*	2.4(1)
T(5)	0.0723(2)	0.0307(3)	−0.1867(4)	8.0	8*d*	2.4(1)
T(6)	0.1922(3)	0.0551(3)	−0.3214(4)	8.0	8*d*	2.4(1)
T(7)	0.4288(3)	−0.1717(3)	−0.3305(4)	8.0	8*d*	2.4(1)
T(8)	0.3123(6)	−0.1268(3)	−0.1796(4)	8.0	8*d*	2.4(1)
T(9)	0.2773(3)	−0.1712(3)	0.0332(4)	8.0	8*d*	2.4(1)
T(10)	0.1218(3)	−0.1717(3)	0.0288(4)	8.0	8*d*	2.4(1)
T(11)	0.0758(3)	−0.1297(3)	−0.1889(4)	8.0	8*d*	2.4(1)
T(12)	0.1956(3)	−0.1734(3)	−0.3157(4)	8.0	8*d*	2.4(1)
O(1)	0.3698(3)	0.0613(5)	−0.2461(5)	8.0	8*d*	3.0(1)
O(2)	0.3115(4)	0.0661(4)	−0.0803(4)	8.0	8*d*	3.0(1)
O(3)	0.1996(4)	0.0588(4)	0.0061(4)	8.0	8*d*	3.0(1)
O(4)	0.0924(4)	0.0615(4)	−0.0821(4)	8.0	8*d*	3.0(1)
O(5)	0.1213(3)	0.0561(4)	−0.2682(5)	8.0	8*d*	3.0(1)
O(6)	0.2440(3)	0.4514(3)	−0.2364(5)	8.0	8*d*	3.0(1)
O(7)	0.3798(3)	−0.1582(4)	−0.2345(5)	8.0	8*d*	3.0(1)
O(8)	0.3070(4)	−0.1592(4)	−0.0746(4)	8.0	8*d*	3.0(1)
O(9)	0.1991(2)	−0.1528(4)	0.0325(5)	8.0	8*d*	3.0(1)
O(10)	0.0918(4)	−0.1649(4)	−0.0807(4)	8.0	8*d*	3.0(1)
O(11)	0.1222(3)	−0.1587(4)	−0.2732(5)	8.0	8*d*	3.0(1)
O(12)	0.2449(3)	−0.1277(3)	−0.2421(5)	8.0	8*d*	3.0(1)
O(13)	0.3307(4)	−0.0483(2)	−0.1611(5)	8.0	8*d*	3.0(1)
O(14)	0.0894(4)	−0.0465(4)	−0.1848(5)	8.0	8*d*	3.0(1)
O(15)	0.4189(3)	0.1285(3)	−0.3916(6)	8.0	8*d*	3.0(1)
O(16)	0.4127(4)	0.0017(3)	−0.4179(4)	8.0	8*d*	3.0(1)
O(17)	0.4038(4)	−0.1300(3)	−0.4225(5)	8.0	8*d*	3.0(1)
O(18)	0.1900(5)	0.1243(3)	−0.3868(5)	8.0	8*d*	3.0(1)
O(19)	0.1901(4)	−0.0070(3)	−0.4048(5)	8.0	8*d*	3.0(1)
O(20)	0.2019(2)	−0.1321(3)	−0.4233(4)	8.0	8*d*	3.0(1)
O(21)	−0.0028(2)	0.0530(4)	−0.2128(5)	8.0	8*d*	3.0(1)
O(22)	−0.0003(2)	−0.1513(4)	−0.2104(5)	8.0	8*d*	3.0(1)
O(23)	0.4267(6)	−0.2500	−0.3560(8)	4.0	4*c*	3.0(1)
O(24)	0.2109(6)	−0.2500	−0.3295(9)	4.0	4*c*	3.0(1)
O(25)	0.2854(6)	−0.2500	0.0631(8)	4.0	4*c*	3.0(1)
O(26)	0.1144(6)	−0.2500	0.0631(8)	4.0	4*c*	3.0(1)
Sb(1)	0.0721(6)	0.2500	0.7729(9)	0.69	4*c*	8.0(1)
Sb(2)	0.3934(6)	0.2500	0.8626(8)	0.69	4*c*	8.0(1)
Sb(3)	0.0044(5)	0.0960(4)	0.5237(8)	1.12	8*d*	8.0(1)
Sb(4)	0.5212(7)	0.2500	0.0370(9)	0.56	4*c*	8.0(1)
O(27)	0.4640(5)	0.2500	0.7365(6)	0.69	4*c*	8.0(1)
O(28)	0.9211(4)	0.2500	0.4903(6)	0.69	4*c*	8.0(1)
O(29)	0.0660(4)	0.1600(4)	0.4550(5)	1.12	8*d*	8.0(1)
O(30)	0.0000	0.0000	0.5000	0.56	4*b*	8.0(1)
H_2O	0.0520(3)	0.1550(4)	0.6650(5)	1.38	8*d*	8.0(1)

Thermal parameters are $U \times 10^2$ Å^2. Population parameters are in terms of the number of atoms per unit cell. The e.s.d. of the least significant figure is given in parentheses. The e.s.d. in the population parameters for antimony atoms, oxygen atoms and water molecules are as follows: Sb(1) 0.001, Sb (2) 0.001, Sb (3) 0.002, Sb (4) 0.002, O (27) 0.001, O (28) 0.001, O (29) 0.002, O (30) 0.002, H_2O 0.016.

Table 3
T–O Bond lengths of the ZSM-5 framework in Sb/ZSM-5

Silicon–oxygen bond lengths in Å			
T(1)–O(1)	1.60(1)	T(7)–O(7)	1.65(1)
T(1)–O(15)	1.61(1)	T(7)–O(17)	1.57(1)
T(1)–O(16)	1.64(1)	T(7)–O(22)	1.59(1)
T(1)–O(21)	1.60(1)	T(7)–O(23)	1.60(1)
T(2)–O(1)	1.56(1)	T(8)–O(7)	1.67(1)
T(2)–O(2)	1.54(1)	T(8)–O(8)	1.56(1)
T(2)–O(6)	1.58(1)	T(8)–O(12)	1.60(1)
T(2)–O(13)	1.67(1)	T(8)–O(13)	1.63(1)
T(3)–O(2)	1.66(1)	T(9)–O(8)	1.59(1)
T(3)–O(3)	1.62(1)	T(9)–O(9)	1.62(1)
T(3)–O(19)	1.57(1)	T(9)–O(18)	1.57(1)
T(3)–O(20)	1.54(1)	T(9)–O(25)	1.63(1)
T(4)–O(3)	1.61(1)	T(10)–O(9)	1.60(1)
T(4)–O(4)	1.58(1)	T(10)–O(10)	1.60(1)
T(4)–O(16)	1.60(1)	T(10)–O(15)	1.60(1)
T(4)–O(17)	1.62(1)	T(10)–O(26)	1.64(1)
T(5)–O(4)	1.59(1)	T(11)–O(10)	1.65(1)
T(5)–O(5)	1.56(1)	T(11)–O(11)	1.58(1)
T(5)–O(14)	1.58(1)	T(11)–O(14)	1.68(1)
T(5)–O(21)	1.62(1)	T(11)–O(22)	1.62(1)
T(6)–O(5)	1.60(1)	T(12)–O(11)	1.61(1)
T(6)–O(6)	1.56(1)	T(12)–O(12)	1.67(1)
T(6)–O(18)	1.64(1)	T(12)–O(20)	1.67(1)
T(6)–O(19)	1.67(1)	T(12)–O(24)	1.57(1)

*T represented Si (Al) of the framework of zeolite HZSM-5 in Tables 2 and 3.

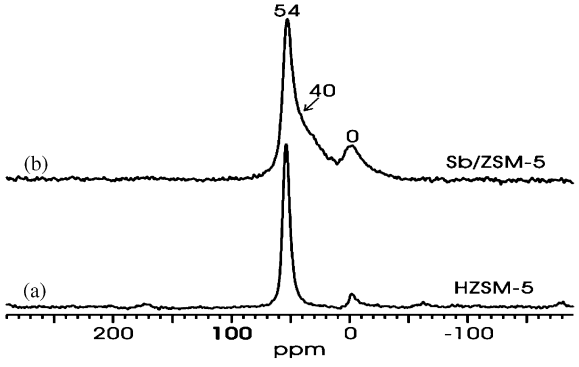

Fig. 1. Al27 MAS NMR profiles of HZSM-5 and Sb/ZSM-5.

3. Result and discussion

3.1. ^{27}Al MAS NMR spectroscopy

The ^{27}Al MAS NMR profile showed that there were two main signals. One signal at 54 ppm is typically associated with tetra-coordinated framework aluminum in zeolite ZSM-5, and the other signal of small intensity at 0 ppm is commonly attributed to octahedral non-framework aluminum [19]. The signal intensity at 54 ppm in the pattern of Sb/ZSM-5 becomes weaker in compared with the parent HZSM-5 (see Fig. 1), and its peak width at half height broadens. It revealed that the framework of zeolite ZSM-5 had some changes during the solid-state reaction, but it still remained the structure of the parent framework. A new peak at about 30–40 ppm, which may be assigned to highly distorted,

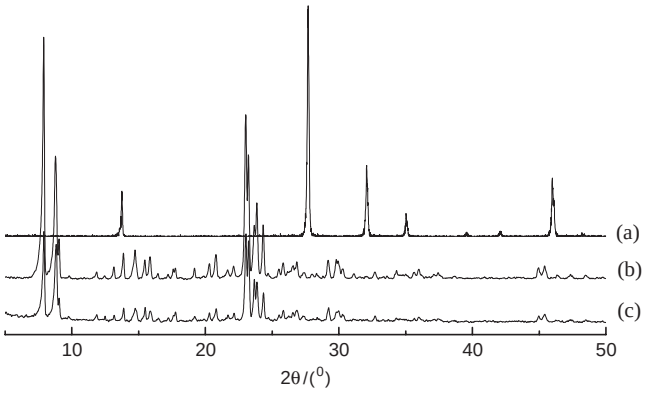

Fig. 2. XRD patterns for the samples: (a) Sb_2O_3 (Senarmontite), (b) ZSM-5 and (c) Sb/ZSM-5.

tetrahedral, non-framework or penta-coordinated aluminum [19], seems to be generated. At the same time, the signal intensity at 0 ppm in the pattern of Sb/ZSM-5 increases. It means some tetra-coordinated aluminum deprived from the framework of zeolite ZSM-5 and became new amorphous penta- and hexa-coordinated aluminum, so the amount of the amorphous phase in calcined sample was higher then before.

3.2. XRD phase analysis

The XRD patterns of the Sb/ZSM-5, HZSM-5 and antimony oxide are shown in Fig. 2. The similarity of the XRD patterns between the HZSM-5 and the modified zeolite indicates that the framework of ZSM-5 was still remained during the reaction. In Fig. 2, crystalline phases of Sb_2O_3 were not detected in the Sb/ZSM-5. Compared with ZSM-5 pattern, the background of the XRD pattern of Sb/ZSM-5 enhanced slightly and the intensities of peaks before 10° 2θ decreased evidently. The increase of the background indicates the increase of the amorphous phase in the Sb/ZSM-5. Since Sb_2O_3 crystallites are not detected by X-ray diffraction, it may indicate that some Sb_2O_3 in small particles (<3 nm) disperse on the external surface of zeolite crystal, or even penetrated into the channels of zeolite ZSM-5 as much smaller species during the treatment as suggested by Zheng et al. [16]. As we known, the low-angle XRD intensities in the pattern of ZSM-5 are sensitive to the presence of any species inside the channels. The decreases of peak intensity of low-angle in the pattern Sb/ZSM-5 also imply the entrance of antimony oxide into the channels.

3.3. BET surface area and microporous volume

BET surface area and microporous volume are presented in Table 4. The BET surface area of the sample shrunk 19% and the microporous volume decreased 20% comparing with the parent ZSM-5.

Table 4
Content, surface area and microporous volume of HZSM-5 and Sb/ZSM-5

Sample	C_{Sb} (wt%)	A_{BET} (m^2/g)	V_m (cm^3/g)
HZSM-5	0	363	0.163
Sb/HZSM-5*	8.35	327	0.147
Sb/ZSM-5	8.07	266	0.117

Sb/HZSM-5*—before calcination, its data comes from calculation, C_{Sb}—the content of Sb, A_{BET}—BET surface area, V_m—microporous volume of samples.

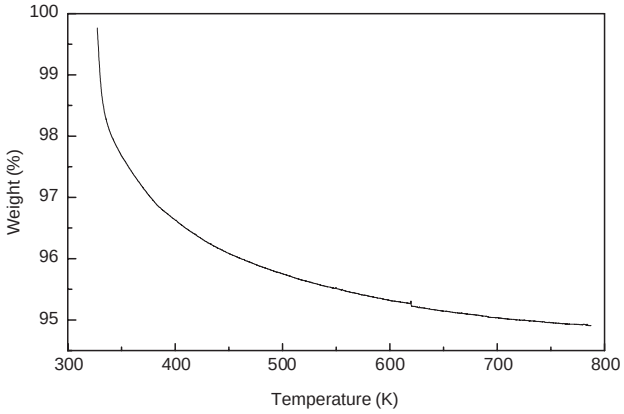

Fig. 3. Relative weight of Sb/ZSM-5, annealed in nitrogen, as a function of temperature.

These changes again implied that some Sb species are well dispersed on the surface and the other Sb species entered into the channels of ZSM-5.

3.4. Thermogravimetric analysis

Fig. 3 shows mass changes of the Sb/ZSM-5 as a function of temperature. In this pattern, the weight decline before 423 K is due to the desorption of physically absorbed water in the surface of ZSM-5, and the weight decline before 623 K is due to the desorption of physically absorbed water inside the channels of ZSM-5 while the weight decline extending to 784 K is due to removal of the structural water and –OH groups via condensation [20]. It indicated that there was some water molecules attached to antimony oxide.

3.5. FT-IR analysis

The curves of FT-IR were shown in Fig. 4. The number of Brönsted and Lewis acid sites was calculated on the basis of the absorbance of the PyB band near 1540 cm^{-1} and the PyL band near 1450 cm^{-1} at 473 K using extinction coefficients ε (PyB) = 0.72 cm^2/mmol and ε (PyL) = 2.37 cm^2/mmol, respectively [21], and the quantitative results were listed in Table 5. The results of

Pyridine-IR confirmed that the number of the Brönsted acid sites in Sb/ZSM-5 decreased remarkably, and they were only 20% of the Brönsted acid sites in the parent HZSM-5. This indicated that some Sb species located at the Brönsted acid sites. In addition, the number of Lewis acid sites increased a little. It may be due to the amphoteric properties of antimony oxide.

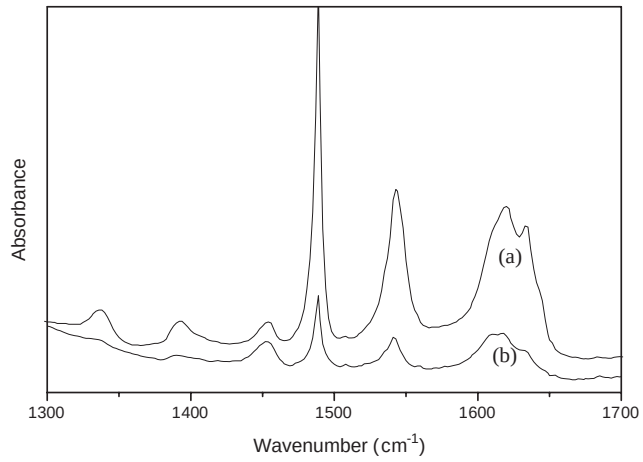

Fig. 4. FT-IR spectra of pyridine adsorbed at 473 K to: (a) HZSM-5 and (b) Sb/ZSM-5.

Table 5
Acid sites number of HZSM-5 and Sb/ZSM-5 determined by Py-IR method

Samples	Brönsted acidity ($\times 10^{20}$/g)	Lewis acidity ($\times 10^{20}$/g)
HZSM-5	8.0	0.2
Sb/ZSM-5	1.6	0.4

3.6. State and distribution of antimony oxide inside channels of ZSM-5

The difference plots for Rietveld structure refinement of the samples was showed in Fig. 5.

As shown in Fig. 6, the antimony oxide distributed inside the channels of ZSM-5 in a chain of non-perfect $[Sb_5O_5(H_2O)_2]_n^{5n+}$. The bond lengths of Sb–O (H_2O) and bond angles in $[Sb_5O_5(H_2O)_2]^{5+}$ are summarized in Table 6.

In its perfect form, every oxygen atom is connected with two antinomy atoms, while antimony atoms are two-coordinated Sb(2) or three-coordinated (Sb(1), Sb(3) and Sb(4)). The water molecules being combined with two antimony atoms (Sb(1), Sb(3)) connect the chain of non-perfect $[Sb_5O_5(H_2O)_2]_n^{5n+}$ with the framework of the zeolite through O(5) atom via hydrogen bond. The distance between the oxygen atom of water molecule and the oxygen atom O(5) is 2.58(1) Å. The main chain –Sb(3)–O(29)–Sb(4)–O(29)–Sb(3)–O(30)– of the non-perfect $[Sb_5O_5(H_2O)_2]_n^{5n+}$ is parallel to the straight channel of ZSM-5 while the atoms Sb(1), Sb(2), Sb(4), which are situated at the cross point of the zigzag channel and the straight channel, extends to the zigzag channel, as shown in Figs. 7 and 8.

The occupancies of Sb atoms and their relating O atoms carried out from XRD structure analysis are around 0.16, which means that there is about 0.6 $[Sb_5O_5(H_2O)_2]^{5+}$ unit in every cell of ZSM-5 on an average. The average electric charges of the chains in each unit cell were 3.0, which neutralized the main part of the electric charges of the framework and to form a relatively stable structure. As a result, Brönsted acidity decreases on a large scale. Accordingly, the content of Sb in crystal phase in Sb/ZSM-5 was 6.0 wt%. Because

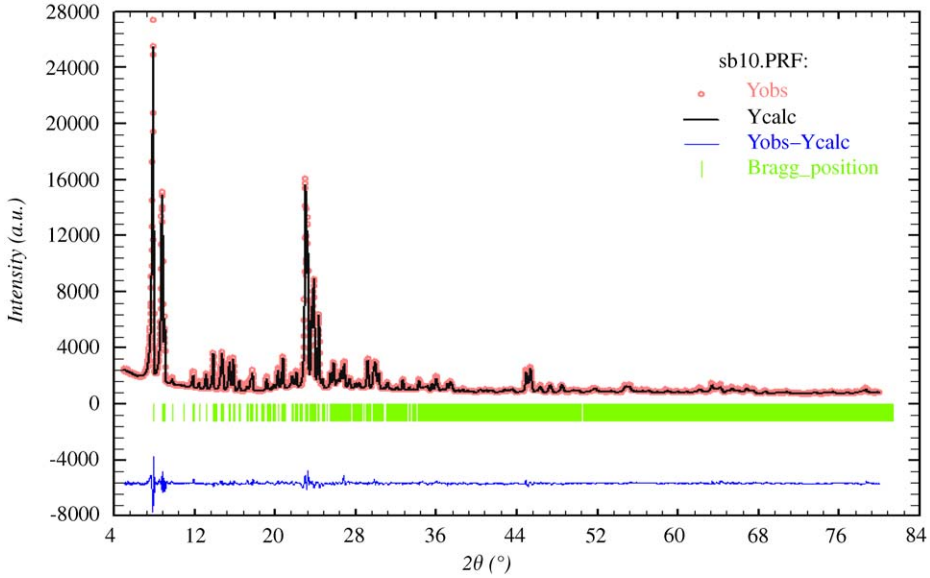

Fig. 5. Observed, calculated and difference plots for Rietveld method structure refinement of Sb/ZSM-5.

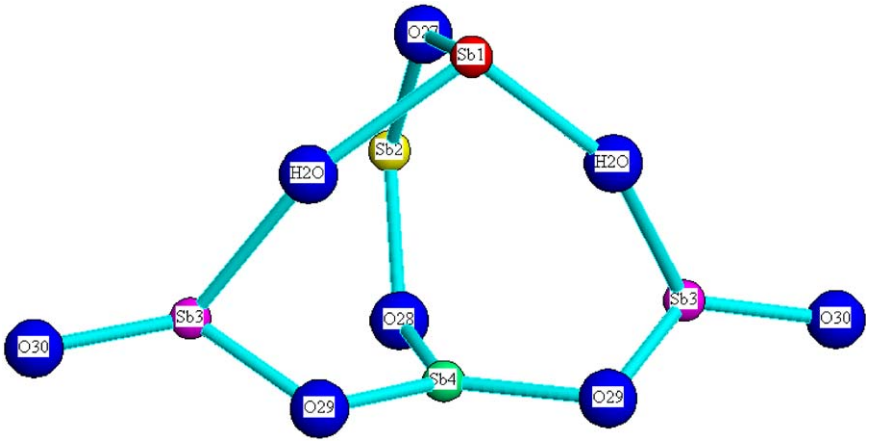

Fig. 6. Description of perfect unit $[Sb_5O_5\ (H_2O)_2]^{5+}$ inside the channels of ZSM-5.

Table 6
Sb–O (H_2O) bond lengths and bond angles in the $[Sb_5O_5\ (H_2O)_2]^{5+}$ unit

Antimony–oxygen bond lengths in Å		Atom 1	−Atom 2	−Atom 3	Angle (deg)
Sb(1)–O(27)	2.18(2)	Sb(1)	–O(27)	–Sb(2)	133.3(6)
Sb(1)–H_2O	2.43(3)	H_2O	–Sb(1)	–H_2O	103.0(3)
Sb(2)–O(27)	2.21(2)	O(27)	–Sb(2)	–O(28)	124.2(5)
Sb(2)–O(28)	2.05(2)	Sb(2)	–O(28)	–Sb(4)	116.0(3)
Sb(3)–O(29)	2.00 (2)	O(28)	–Sb(4)	–O(29)	116.7(4)
Sb(3)–O(30)	1.94 (2)	O(29)	–Sb(4)	–O(29)	126.4(4)
Sb(3)–H_2O	2.43(3)	H_2O)	–Sb(3)	–O(30)	128.5(5)
Sb(4)–O(28)	2.05(3)	Sb(4)	–O(29)	–Sb(3)	105.4(6)
Sb(4)–O(29)	2.01(1)	O(29)	–Sb(3)	–O(30)	125.4(5)
Sb(4)–O(29)	2.01(1)	Sb(3)	–O(30)	–Sb(3)	180

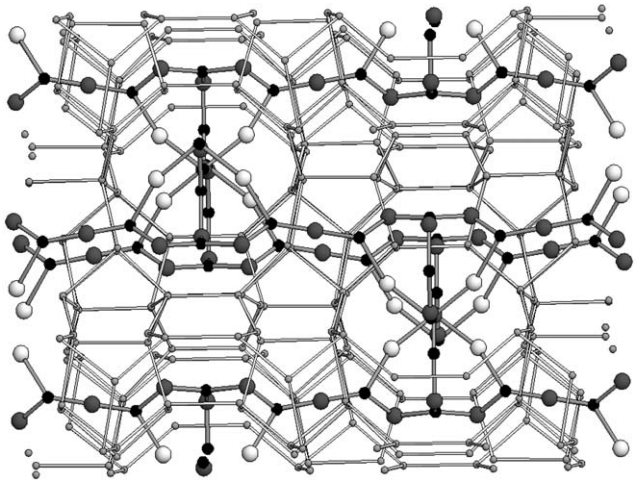

Fig. 7. Distribution of perfect unit $[Sb_5O_5\ (H_2O)_2]_n^{5n+}$ inside the channels of ZSM-5 projected along the (100) direction with framework.

the ratio of Sb_2O_3 to HZSM-5 with 91% crystallinity is 1:9, there is 82% (90*91%) crystallinity of the ZSM-5 in the initial mixture, which means that the part of Sb species modified the channels of the zeolite is about 4.92 wt% accounting on the whole sample. The chemical analysis shows that the content of Sb is 8.07 wt%, there is about 3.15 wt% Sb species excess. It reveals that part of antimony oxides should mix with the amorphous alumino-silicate oxides, distribute on the external surface of zeolite ZSM-5 and modify it.

4. Conclusions

Sb/ZSM-5 was prepared by solid-state with the mixture of Sb_2O_3 and zeolite HZSM-5 under a dry nitrogen flow at 773 K for 2 h. The characterization of the Sb/ZSM-5 confirmed that the framework of Sb/ZSM-5 is as the same as that of the parent HZSM-5. One part of antimony oxides migrated into the

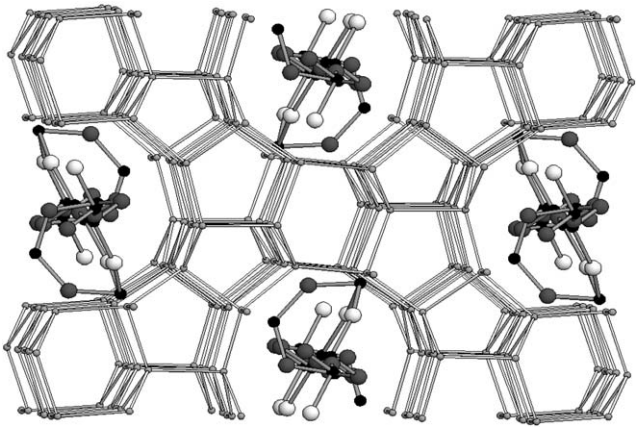

Fig. 8. Distribution of perfect unit $[Sb_5O_5\ (H_2O)_2]_n^{5n+}$ inside the channels of ZSM-5 projected along the (010) direction with framework.

channels of ZSM-5, the other part of antimony oxides together with amorphous alumino-silicate oxides distributed on the external surface of zeolite. As a result, the acidic center of the zeolite ZSM-5 was harbored, and the Brönsted acid sites decreased obviously. By contraries, the amount of Lewis acid sites increased slightly. Rietveld method analysis revealed that the structure of antimony oxide species can be described as a non-perfect chain $[Sb_5O_5\ (H_2O)_2]_n^{5n+}$, which is parallel to the straight channel of ZSM-5. There is about 0.6 $[Sb_5O_5(H_2O)_2]^{5+}$ unit in every cell of ZSM-5 on an average.

Acknowledgments

The authors are grateful for the financial support from NSFC (contract No. 20373002).

References

[1] R.J. Argauer, G.R. Landolt, Crystalline Zeolite ZSM-5 and Method of Preparing the same, US Patent 3,702,886, 1972.
[2] G.T. Kokotail, S.L. Lawton, D.H. Olson, W.M. Meier, Nature (London) 272 (1978) 437.
[3] D.H. Olson, G.T. Kokotailo, S.L. Lawton, W.M. Meier, J. Phys. Chem. 85 (1981) 2238.
[4] Z.-Y. Liu, W.-J. Zhang, Q. Yu, G.-L. Lu, W.-R. Li, S.-J. Wang, B.-X. Lin, Distrbution of the bivalent nickel ion in ZSM-5 molecular sieves, in: Y. Murakaimi, A. lijima, J.W. Ward (Eds.), Proceeding of the Seventh International Zeolite Conference, Yokyo, Japan, August 17–22. Kodansha Elsevier, Tokyo, 1986, p. 415.
[5] D.H. Katherine, L.V.C. Rees, Zeolites 11 (1991) 270.
[6] A.V. Kucherov, T.N. Hucherova, A.A. Slinkin, Microporous Mesoporous Mater. 26 (1998) 1.
[7] A.A. Slinkin, A.V. Kucherov, Catal. Today 36 (1997) 485.
[8] H.K. Beyer, G. Pal-Borbely, M. Keindl, Microporous Mesoporous Mater. 31 (1999) 333.
[9] H.G. Karge, H.K. Beyer, Zeolite Chemistry and Catalysis, Elsevier, Amsterdam, 1991, p. 43.
[10] S. Beran, B. Wichterlova, H.G. Karge, J. Chem. Soc. Faraday Trans. I 86 (1990) 3033.
[11] J. Thoret, C. Doremieux-Morin, P.P. Man, M. Gruia, J. Fraissard, Zeolites 13 (1993) 269.
[12] J. Thoret, P.P. Man, J. Fraissard, J. Chem. Soc. Faraday Teans. 91 (1995) 1037.
[13] J. Thoret, P.P. Man, J. Fraissard, Zeolites 18 (1997) 152.
[14] J. Thoret, P.P. Man, P. Ngokoli-Kekele, J. Fraissard, Microporous Mesoporous Mater. 49 (2001) 45.
[15] G.Y. Li, J.C. Zhao, Petrochen. Technol. (Chinese) 16 (1987) 272 (In Chinese).
[16] S. Zheng, A. Jentys, J.A. Lercher, J. Catal. 219 (2003) 310.
[17] Z.-Y. Liu, S.-J. Wang, W.-R. Li, W.-J. Zhang, Acta Petrolei Sinica (Petroleum Processing Section) 2 (1985) 39 (In Chinese).
[18] T. Roisnel, J. Rodriguez-Carvajal, http://www-llb.cea.fr/fullweb/winpotr.
[19] S.M. Campbell, D.M. Bibby, J.M. Coddington, R.F. Howe, R.H. Meinhold, J. Catal. 161 (1996) 338.
[20] B. Ganemi, E. Björnbom, B. Demirel, J. Paul, Microporous Mesoporous Mater. 38 (2000) 287.
[21] L. Kubekková, S. Beran, A. Malecka, V.M. Mastikhin, Zeolites 9 (1989) 12.